ORNL/TM-2022/2675

Design and Scoping Tests on Alloy 617 Using Notched Specimen Geometry to Validate Methods for Multiaxial Stress Relaxation

Yanli Wang
Peijun Hou

September 2022

OAK RIDGE National Laboratory

ORNL IS MANAGED BY UT-BATTELLE LLC FOR THE US DEPARTMENT OF ENERGY

ORNL/TM-2022/2675

Materials Science and Technology Division

DESIGN AND SCOPING TESTS ON ALLOY 617 USING NOTCHED SPECIMEN GEOMETRY TO VALIDATE METHODS FOR MULTIAXIAL STRESS RELAXATION

Yanli Wang
Peijun Hou[1]

[1]Imtech Corporation, Knoxville

Date Published: September 2022

Prepared by
OAK RIDGE NATIONAL LABORATORY
Oak Ridge, TN 37831
managed by
UT-BATTELLE LLC
for the
US DEPARTMENT OF ENERGY
under contract DE-AC05-00OR22725

Page intentionally left blank.

CONTENTS

LIST OF FIGURES

LIST OF TABLES

ABBREVIATIONS

ASME	American Society of Mechanical Engineers
BPVC	Boiler and Pressure Vessel Code
CF	creep-fatigue
DOE	US Department of Energy
ORNL	Oak Ridge National Laboratory
FE	finite element

ACKNOWLEDGMENTS

This research was sponsored by the US Department of Energy (DOE) under contract no. DE-AC05-00OR22725 with Oak Ridge National Laboratory (ORNL), managed and operated by UT-Battelle LLC. Programmatic direction was provided by the Office of Nuclear Reactor Deployment of the DOE Office of Nuclear Energy.

The authors gratefully acknowledge the support provided by Sue Lesica, Federal Materials Lead for the Advanced Reactor Technologies (ART) Program; Matthew Hahn, Federal Program Manager of the ART Gas-Cooled Reactors (GCR) Campaign; Gerhard Strydom of Idaho National Laboratory, National Technical Director of the ART GCR Campaign, and T.-L. Sham of Idaho National Laboratory, Technology Area Lead, Advanced Materials, ART Program.

The authors also wish to thank ORNL staff members Lianshan Lin and Jian Chen for reviewing this report.

Page intentionally left blank.

ABSTRACT

In FY 2022, a development effort was initiated at the US Department of Energy's Oak Ridge National Laboratory (ORNL) to examine the multiaxial stress-relaxation behavior and multiaxial stress-state effect on the creep-fatigue (CF) performance for Alloy 617 at elevated temperatures. This effort supported the development of the design rules in the American Society of Mechanical Engineers (ASME) Boiler and Pressure Vessel Code (BPVC), Section III, Division 5. In this work, two types of the notch specimen geometries were designed. An inelastic constitutive model was used to investigate the stress triaxiality and elastic follow-up effects on the notch specimens under CF deformation in the finite element (FE) simulations. The numerical study demonstrated that the stress triaxiality and elastic follow-up caused by the notches both play significant roles in the stress-relaxation behavior. In addition, Alloy 617 CF experiments were designed, and the testing on the notch specimens is ongoing. CF test failure data will be generated on the specimens with notches under various conditions in FY 2023, and the results will be used to validate methods for accounting for the multiaxial stress relaxation effect in the design code.

1. INTRODUCTION

CF interactive damage at elevated temperatures is the most damaging mode for structural components under cyclic loading. In the past several decades, researchers have devoted considerable effort to the elevated temperature code rule development in the ASME BPVC, Section III, Division 5 to ascertain conservative structural designs against CF failure. Advances in the CF performance of the structural materials and the CF evaluation rules are essential to enhance the economics of high temperature reactors.

In practice, reactor structural components are often under the complex multiaxial CF loading conditions throughout the lifetime because of geometric or metallurgical discontinuities and complicated loading paths. An accurate description of the multiaxial stress-relaxation behavior at critical locations is desired for developing CF evaluation rules in the design code. The purpose of this study is to design CF experiments under multiaxial loading and to collect critical information to evaluate the effect of multiaxial stress state on CF.

To this end, Alloy 617 (UNS N06617) was selected as the focus of this study. Alloy 617 has been approved for elevated temperature service construction of Class A components conforming to the requirements of the ASME BPVC Section III, Division 5, Subsection HB, Subpart B "Elevated Temperature Service," for service temperature up to 1,750°F (954°C) and service life up to 100,000 h, via Code Case N-898 in 2019. Relevant CF testing data on standard smooth bar specimens (Wright 2021) and a limited number of tests with elastic follow-up (Hou et al. 2022; Wang et al. 2016a, 2016b, 2017a, 2017b, 2018, 2019, 2020, 2021a, 2021b, 2022) are available to the research team to use as the baseline for comparison. In this study, an inelastic constitutive model was used to investigate the effect of notches under CF deformation in the FE simulations. The numerical results are summarized in this report, and they provide an understanding of multiaxial stress-relaxation behavior caused by geometric discontinuities on the CF loading. During this report period, experimental CF tests for the notch specimens were designed and test to failure data will be generated. The experimental results and the comparison with standard uniaxial CF tests will be conducted in FY 2023.

2. FINITE ELEMENT SIMULATION OF NOTCH SPECIMEN UNDER CREEP-FATIGUE DEFORMATION

2.1 ALLOY 617 NUMERICAL INELASTIC MODEL

In this work, a numerical inelastic model involves the isotropic hardening rule describing the time-independent cyclic plastic deformation and the time-dependent power-law creep rule describing the stress-relaxation behavior at hold-time period under CF loading conditions. The small deformation and initial isotropic elasticity are assumed in this model. The main governing equations of the constitutive model are outlined as follows.

The total strain increment $d\varepsilon_{ij}^{t}$ can be decomposed and expressed as Eq. (1):

$$d\varepsilon_{ij}^{t} = d\varepsilon_{ij}^{e} + d\varepsilon_{ij}^{p} + d\varepsilon_{ij}^{c} \tag{1}$$

where ε_{ij}^{e} is the elastic strain, ε_{ij}^{p} is the time-independent plastic strain, and ε_{ij}^{c} is the time-dependent creep strain.

The constitutive relationship between the stress, σ_{ij}, and the elastic strain, ε_{ij}^{e}, is expressed by the generalized Hook's law:

$$d\varepsilon_{ij}^{e} = D_{ijkl} : d\sigma_{kl} \tag{2}$$

where D_{ijkl} is the elastic compliance tensor. The Von Mises yield criterion was used to simulate the plastic flow in the mechanical analysis, given by Eq. (3):

$$f(\sigma_{ij}, R) = \sqrt{\frac{3}{2} S_{ij} : S_{ij}} - R(\bar{\varepsilon}^{p}) \tag{3}$$

where S_{ij} is the component of the deviatoric stress tensor, and R denotes the deformation resistance. The equivalent plastic strain, $\bar{\varepsilon}^{p}$, is determined from the condition for which the Von Mises yield criterion is satisfied, and the equivalent plastic strain increment, $d\bar{\varepsilon}^{p}$, is

$$d\bar{\varepsilon}^{p} = \sqrt{\frac{2}{3} d\varepsilon_{ij}^{p} : d\varepsilon_{ij}^{p}} \tag{4}$$

The isotropic hardening model is used to describe the hardening behavior, given by Eq. (5):

$$R = \sigma_{Y} + Q\left(1 - e^{-b\bar{\varepsilon}^{p}}\right) \tag{5}$$

where σ_{Y} is the initial cyclic yield stress, and Q and b describe the isotropic strain hardening behavior.

The creep deformation is described by a power-law model and is expressed as Eq. (6):

$$\frac{d\bar{\varepsilon}^{c}}{dt} = A\sigma_{e}^{n} \tag{6}$$

where $\bar{\varepsilon}^c$ is the equivalent creep strain, σ_e is the von Mises stress ($\sigma_e = \sqrt{\frac{3}{2} S_{ij} : S_{ij}}$), and n is the stress exponent. The equivalent creep strain increment is given by Eq. (7):

$$d\bar{\varepsilon}^c = \sqrt{\frac{2}{3} d\varepsilon_{ij}^c : d\varepsilon_{ij}^c} \tag{7}$$

The elastic modulus E and initial yield stress σ_Y can be obtained from the uniaxial tensile data for Alloy 617 at 950°C. Poisson's ratio ν is assumed to be 0.3. The commercial software ABAQUS was used to automatically determine the material parameters Q and b in the isotropic hardening rule by fitting the uniaxial tensile curve. The material parameters A and n in the power-law creep equation were determined using previous 600 s tensile-hold CF data for Alloy 617 at 950°C (Wright 2021). The material parameters used in this study are listed in Table 1.

Table 1. Material parameters in the numerical inelastic model of Alloy 617 at 950°C

Parameters	Value
E	136 GPa
υ	0.3
σ_Y	155 MPa
A	5.12218×10^{-16}
n	5.6

2.2 FINITE ELEMENT SIMULATION FOR NOTCH SPECIMENS

An axisymmetric FE model for the uniform and notch specimens was built using the commercial software ABAQUS Standard to calculate the stress field, strain field, and strain energy field under nominal strain range of 0.6% and tensile hold time of 600 s. Two types of notch specimens were employed in this study: shallow-notch and V-notch. The dimensions of the notch geometries are same as those for the experiments, which are described in *Section 3*. The specimen diameter is 0.5 in. (6.35 mm). The two types notch specimen designs follow the ASTM Standard E292-09. The ratio of the outer diameter to inner diameter in both shallow-notch and V-notch specimens is approximately $\sqrt{2}$, which is recommended by the Code of Practice (ASTM E292-09). The axisymmetric model is established according to the axial symmetric geometry of the specimen and the axial loading condition. In addition, 0.5 in. (12.7 mm) length and 0.75 in. (19.05 mm) in the gauge section for each notch specimen were simulated in the FE model with the purpose of comparison to experimental data as the extensometers used in the experimental CF tests described in *Section 3* having two nominal gauge lengths of 0.5 in. (12.7 mm) and 0.75 in. (19.05 mm). Note that specimens in the FE model were subjected to a global displacement-controlled loading waveform with a total nominal strain range of 0.6%, as illustrated in Figure 1. The effect of strain rate on loading and unloading periods are not included in this simulation work, and the time of the loading and unloading stage 1, stage 3, stage 4, and stage 5 in the loading waveform is 1 s. In this report, the numerical results of the FE model of the 0.5 in. gauge section are mostly presented in *Section 2.3* to provide a basic understanding of notch effect on the stress and strain distributions, and the results of the 0.75 in. gauge length FE model are only used to investigate the influence of geometric size on the elastic follow-up by comparing the calculated elastic follow-up values between 0.5 in. gauge length and 0.75 in. gauge length models. The meshing and boundary conditions of the uniform, shallow-notch, and V-notch specimens with the gauge section of 0.5 in. are shown in Figure 2. The element type used is a four-node bilinear brick element (CAX4 in ABAQUS), and the lateral length of each element near notch root and notch boundaries is approximately 0.002 mm. The bottom surfaces in FE models were fixed in the *y* direction (i.e., $u_y = 0$).

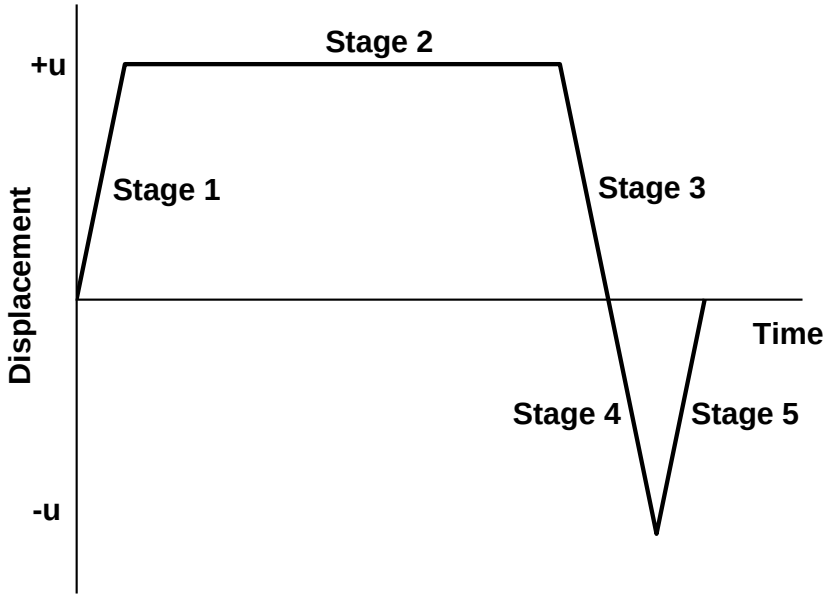

Figure 1. Displacement-controlled CF loading profile for one cycle in FE model.

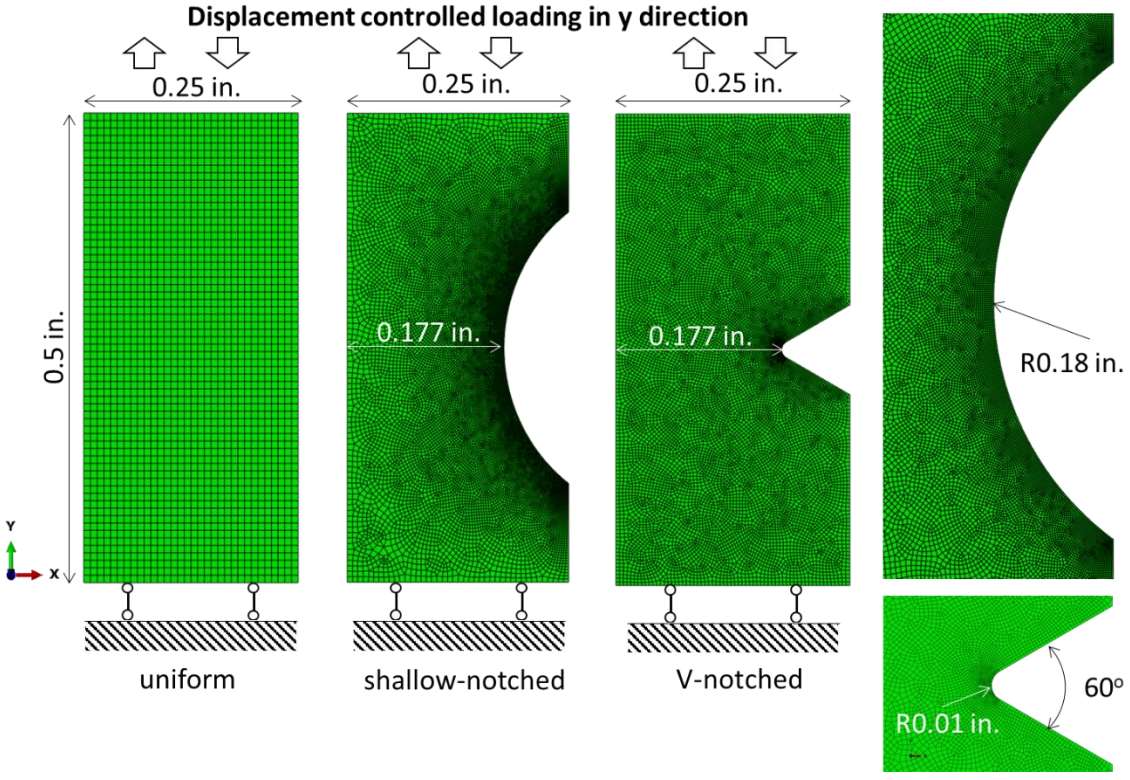

Figure 2. FE model, meshing, boundary conditions, and dimensions of the uniform and notch specimens.

2.3 NUMERICAL RESULTS

2.3.1 UNIAXIAL UNIFORM SMOOTH BAR SPECIMEN

Figure 3 shows the comparison in cyclic stress strain curves from the FE model of a uniaxial uniform specimen (with 20 cycles calculated) and the previous experimental CF test at strain range of 0.6% with 600 s tensile hold time for Alloy 617 at 950°C. Also shown are the global cyclic stress strain curves of the shallow-notch specimen and the V-notch specimen from the FE model. Because of the instability in the strain range at initial cycles in experimental data, only the experimental results at the 10th and 20th cycles are presented and compared to the simulation results in Figure 3. Figure 4 compares the stress relaxation curves at the 10th and 20th cycles. As shown in Figure 3 and Figure 4, a good agreement between experiments and the simulations has been achieved. In addition, the global stress-relaxation curves in the notch specimens are normalized by initial stress during hold time stage and the results are presented for 1st and 10th cycles in Figure 4 along with the corresponding curve from the uniform specimen. The stress-relaxation rate is lower in the notch specimens compared to that in the uniform specimen.

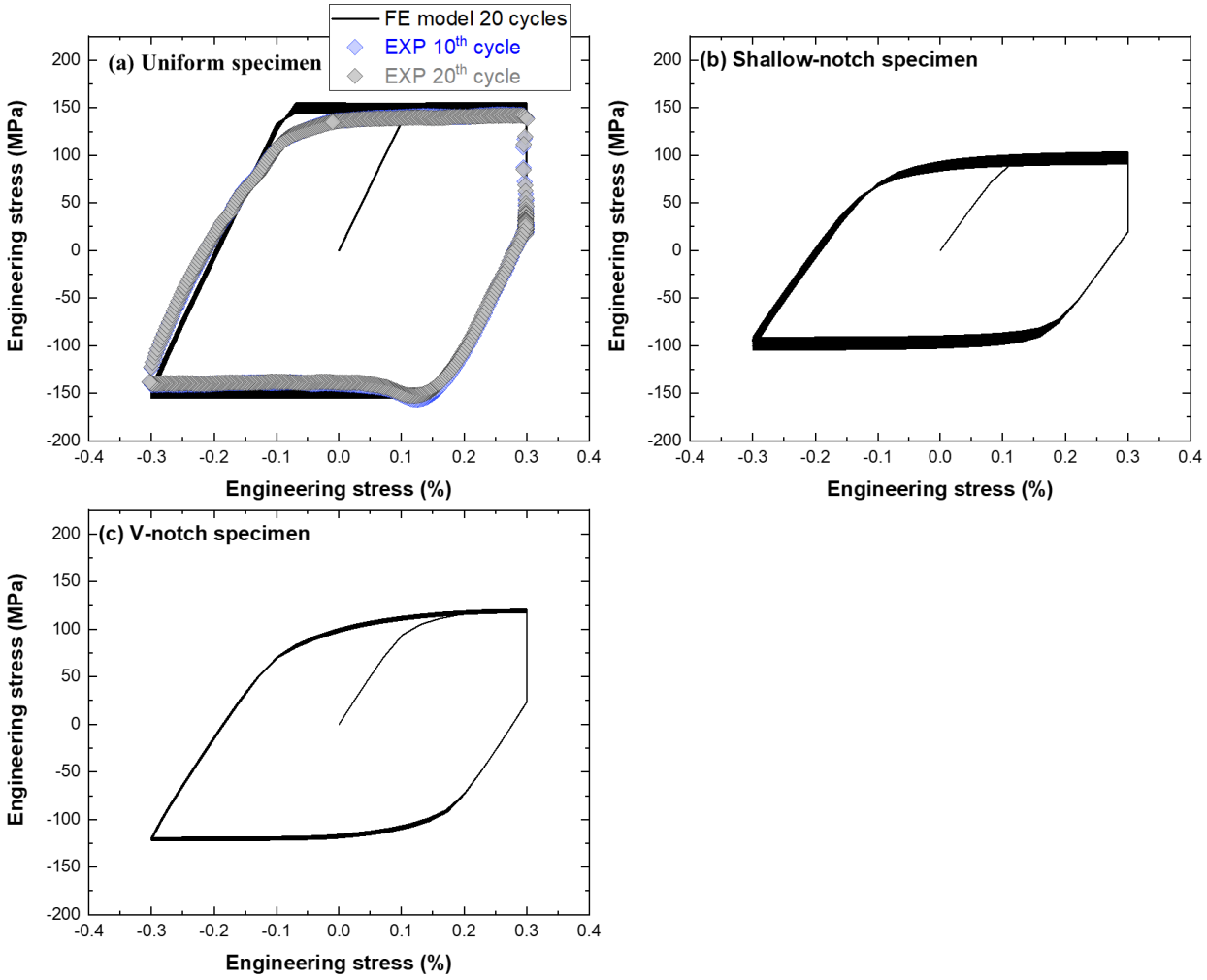

Figure 3. Experimental creep-fatigue data at the 10th and 20th cycles, and simulation results of the global hysteresis loops at the initial 20 cycles. (a) Uniaxial uniform specimen, (b) shallow-notch specimen, and (c) V-notch specimen.

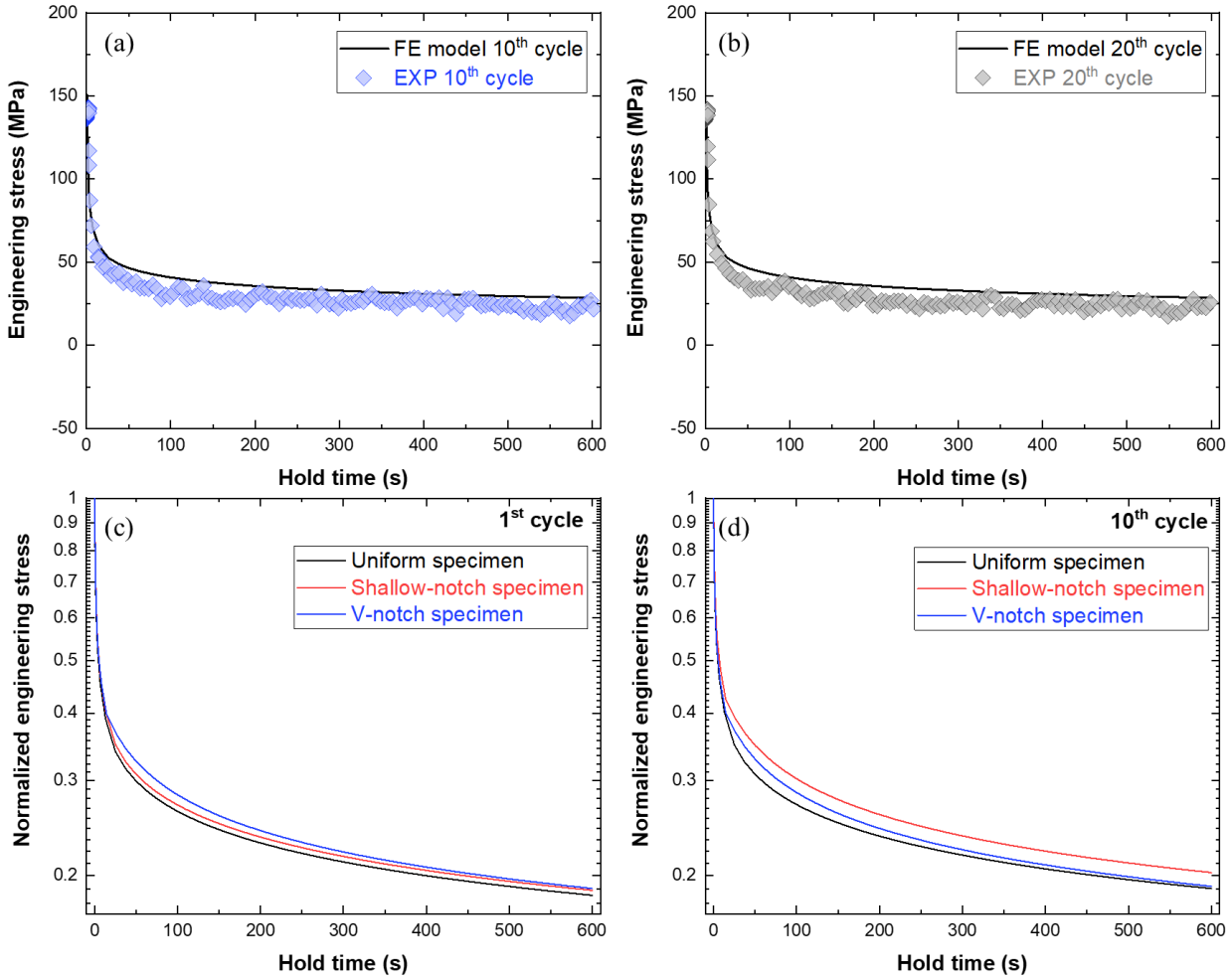

Figure 4. Experimental data and simulation results of stress-relaxation curves at (a) the 10th cycle and (b) the 20th cycle. Global normalized stress-relaxation curves calculated in the notch specimens and uniform specimen at (c) the 1st cycle and (d) the 10th cycle.

Figure 5 shows the calculated stress at the end of loading stage 1 at the first cycle using the inelastic constitutive model (with the creep effect) for uniaxial uniform specimen in comparison to the stress calculated using a time-intendent elastic-plastic model without creep deformation. The model correctly captures the creep effect and the creep deformation lowers the calculated stress from about 154 MPa to 147 MPa. The numerical study and analysis in the following sections have incorporated the creep effect.

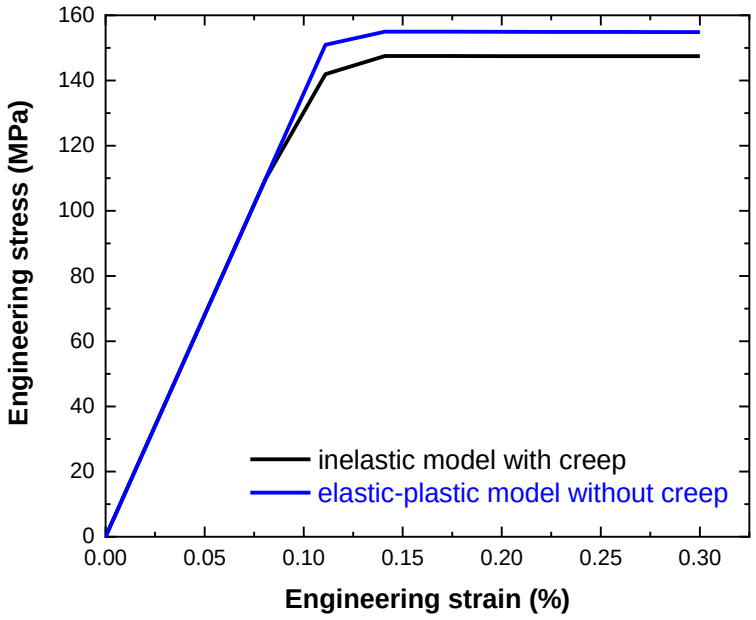

Figure 5. The calculated stress at the end of loading stage 1 at the 1st cycle for the uniaxial uniform specimen. (a) Stress calculated using the inelastic model with creep effect, and (b) a time-independent elastic-plastic model without the creep deformation.

2.3.2 CALCULATED RESULTS OF DISTRIBUTION OF STRESS, STRAIN, AND STRESS TRIAXIALITY

Figure 6 and Figure 7 show the von Mises stress and maximum principal stress contours of the 0.5 in.-gauge-length notch specimens at end of each loading stage (i.e., five stages in the tension-hold trapezoidal loading waveform, as illustrated in Figure 1) at 1st and 10th cycles, respectively. As expected, the distribution of the von Mises stress is affected by the notch geometry and the applied cycles. However, the effect of the accumulated cyclic loading on the distribution of von Mises stress is not significant. The von Mises stress at the end of the hold-time period is subjected to a large relaxation due to the creep deformation. The principal stress is larger than the von Mises stress. As the cycle number increases, the maximum principal stress decreases.

To study the multiaxial stress effect, the stress triaxiality factor, STF, distribution is calculated according to Eq. (8) and is presented at the initial loading (stage 1 in loading waveform, as shown in Figure 1) and holding period (stage 2 in loading waveform, as shown in Figure 1) in Figure 8.

$$STF = \frac{\sigma_m}{\sigma_e} = \frac{\frac{1}{3}\sigma_{ii}}{\sqrt{\frac{3}{2}S_{ij}S_{ij}}} \tag{8}$$

where σ_m denotes the hydrostatic stress and σ_e is the von Mises equivalent stress. At the end of the loading stage (stage 1), the STF is higher at the vicinity of the notch in the V-notch specimen than that in the shallow-notch specimen. The maximum stress triaxiality is located at the center of the shallow-notch

specimen but about 0.4 mm away from the notch root for this V-notch specimen. The stress triaxiality in notch specimens changes with increased CF loading cycles. For example, in the shallow-notch specimen, the *STF* at the end of the hold-time period ranged from −0.3 to 1.2 at the 1st cycle, and the maximum value increased to 1.4 at the 10th cycle, whereas, the *STF* in the V-notch specimen ranges from −0.8 to 1.5 at the end of holding at the 1st cycle, and changed to a range of−0.9 to 1.4 and the 10th cycle.

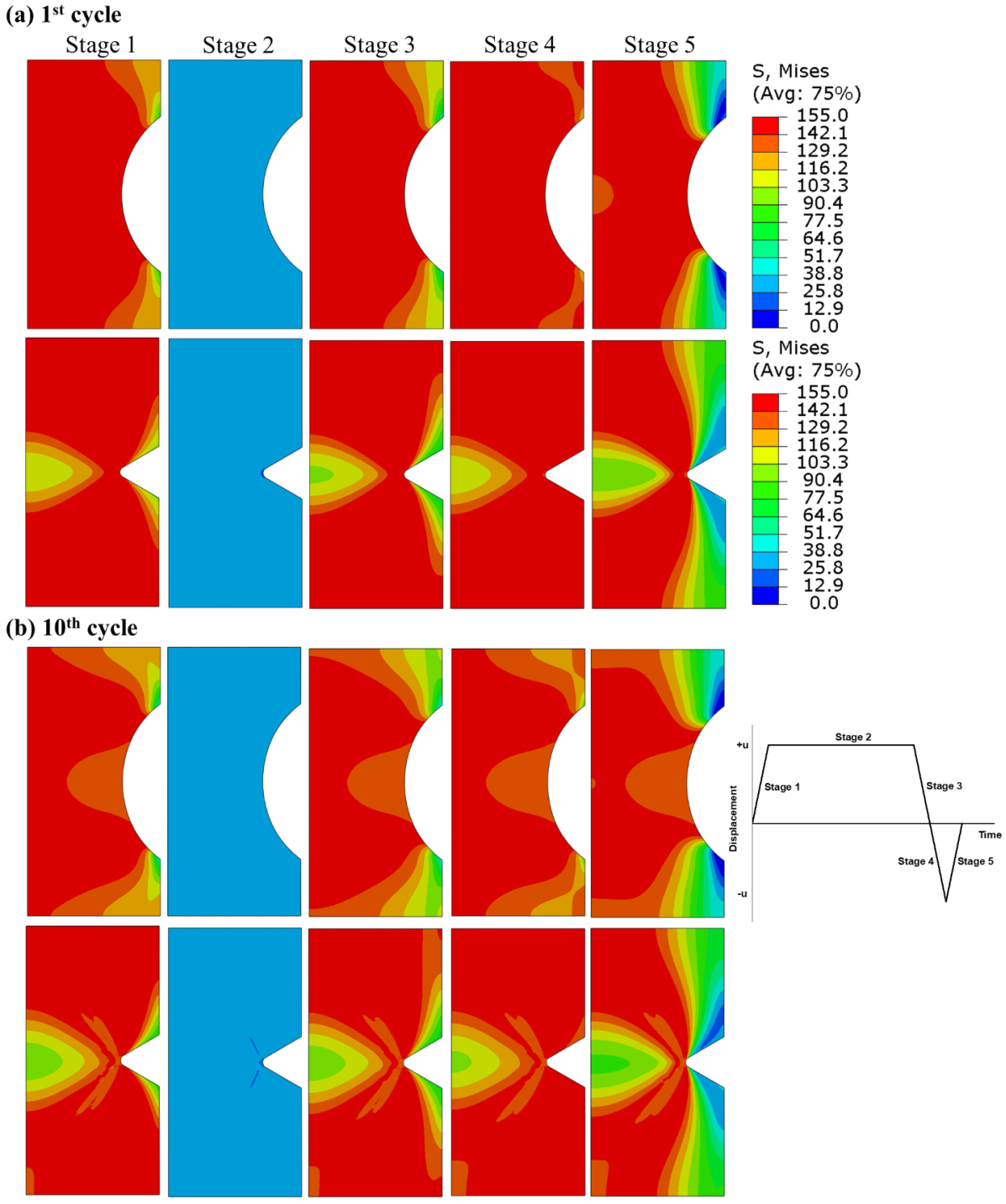

Figure 6. The contours of von Mises equivalent stress at the end of stage 1, stage 2, stage 3, stage 4, and stage 5 for the shallow- and V-notch specimens. (a) 1st cycle and (b) at the 10th cycle.

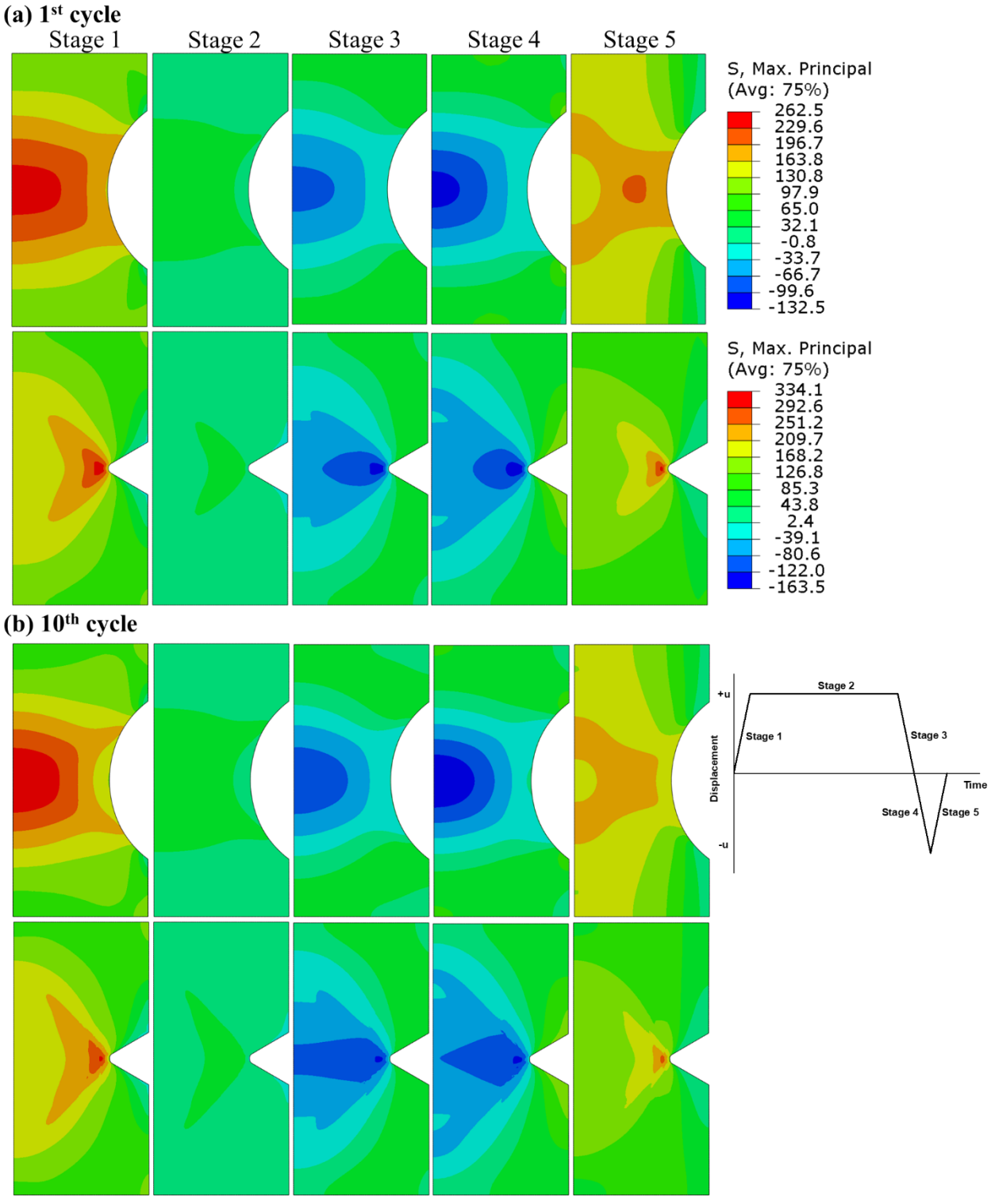

Figure 7. The contours of principal stress at the end of stage 1, stage 2, stage 3, stage 4, and stage 5 for the shallow- and V-notch specimens. (a) 1st cycle and (b) the 10th cycle.

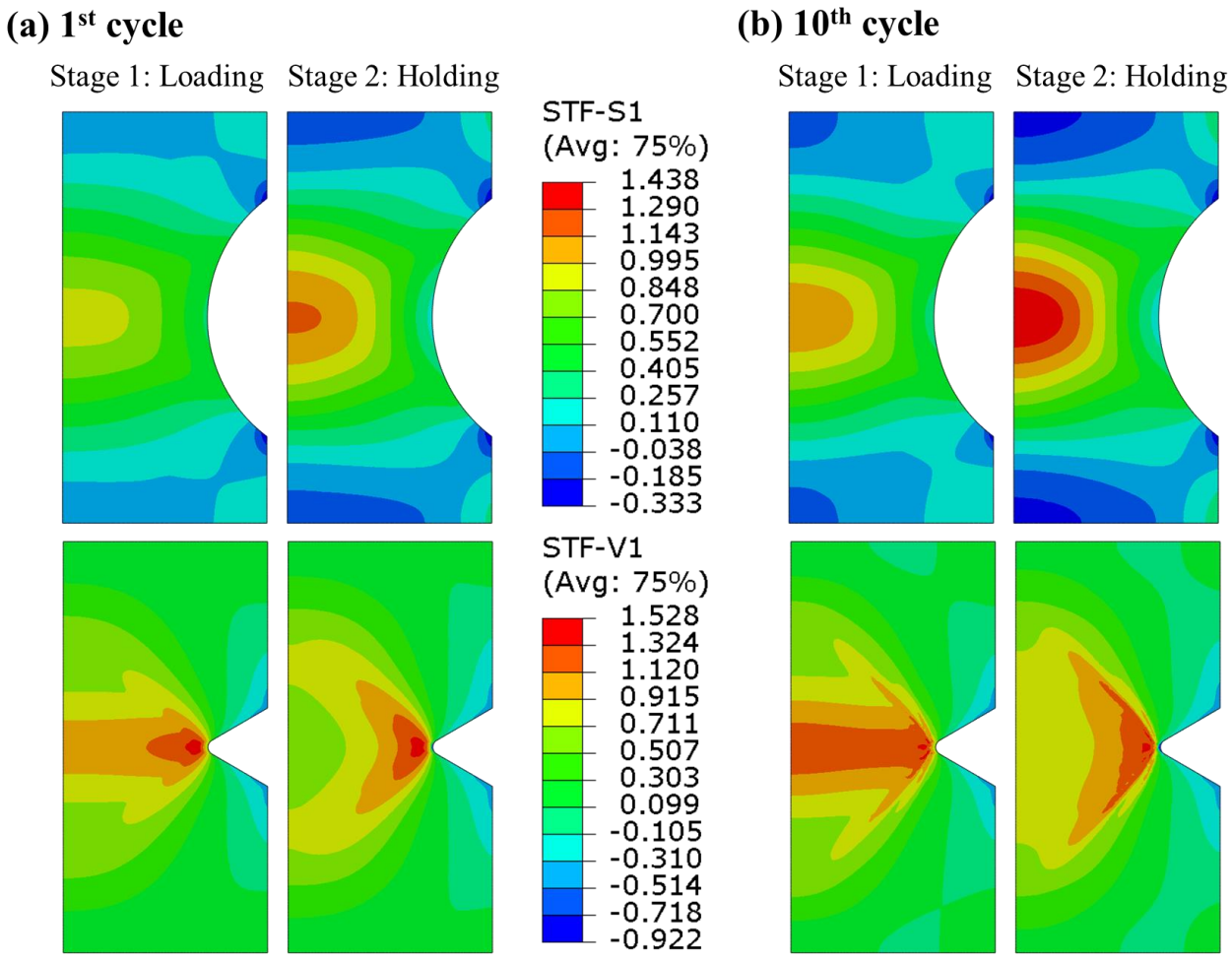

Figure 8. The contours of stress triaxiality factor at the end of loading (stage 1) and holding (stage 2) for the shallow- and V-notch specimens. (a) 1st cycle and (b) 10th cycle.

The equivalent plastic strain contours are presented in Figure 9 for the notch specimens at different loading stages at 1st and 10th cycles. The V-notch specimen has much higher maximum equivalent plastic strain than the shallow-notch specimen but localized at the root of the notch as compared to the shallow-notch condition at the same loading stages. This analysis provides insights in assessing the dominating failure mechanism in the CF evaluation since the plastic strain accumulation is closely to fatigue damage.

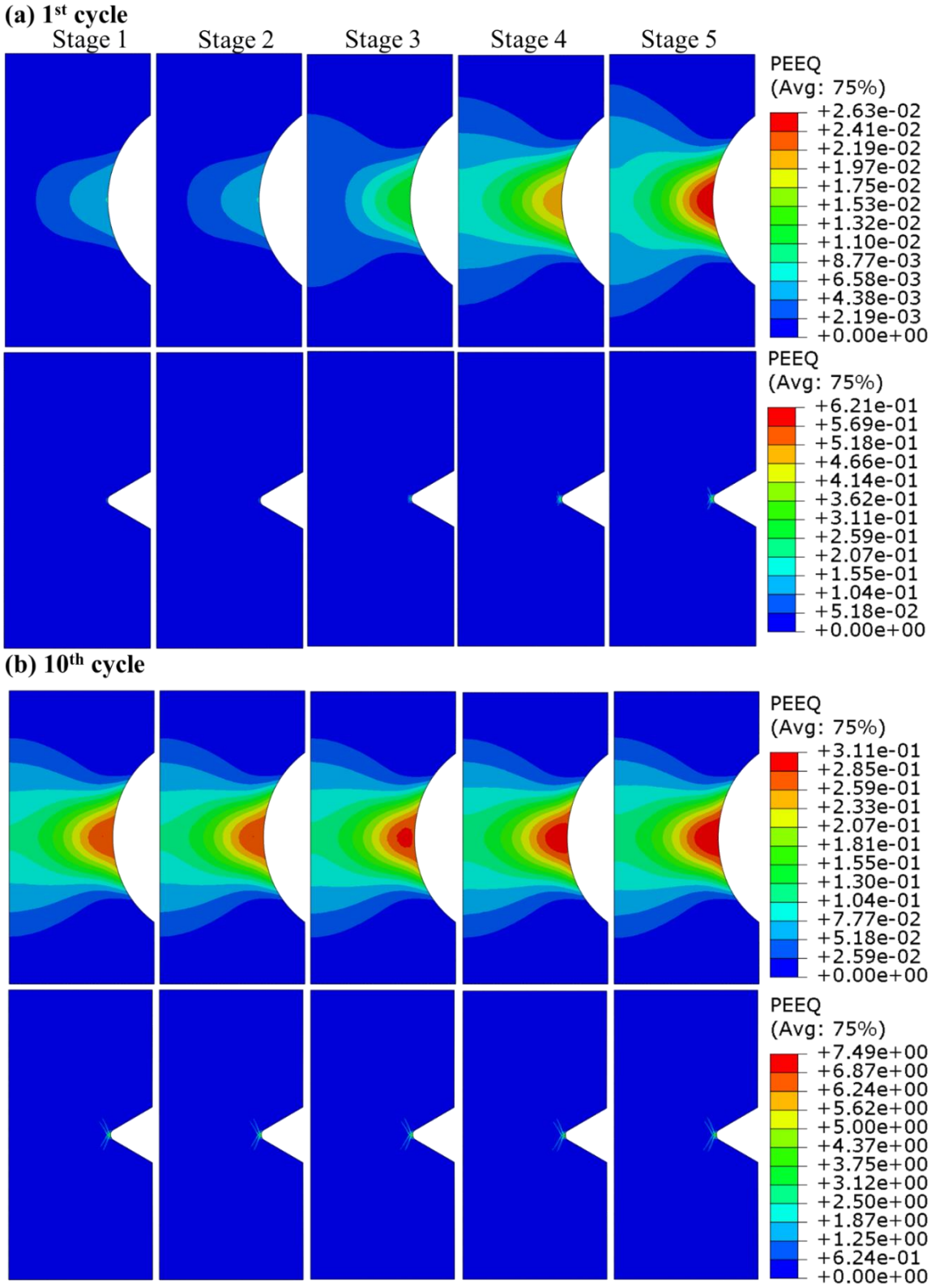

Figure 9. The contours of equivalent plastic strain at the end of stage 1, stage 2, stage 3, stage 4, and stage 5 for the shallow- and V-notch specimens. (a) 1st cycle and (b) 10th cycle.

Figure 10 shows the equivalent creep strain contours for the uniform specimen and notch specimens of 0.5 in. gauge length at the end of the hold at 1st and10th cycles, respectively. As shown in this figure, the notch leads to a higher maximum creep strain than the uniform specimen for both notch geometries. The V-notch specimen exhibits higher maximum accumulated creep strain than the shallow-notch specimen, although the locations of the maximum creep strain relative to the notches are different. In addition, the creep rates at the 10th cycle in the uniaxial uniform, shallow-notch and V-notch specimens of 0.5 in. gauge section were calculated in each element in FE models, as shown in Figure 11. Note that the creep strain rate in Figure 11 was calculated based on the changes in the equivalent creep strain from the initial 10 s of the hold-time. The uniform specimen shows a uniform distribution of the equivalent creep strain rate with a value of 2.21×10^{-5} /s. Both notch specimens showed higher creep strain rates than the uniform specimen. The locations with maximum creep strain rate are marked in this figure and the locations relative to the root of the notch are different for the two geometries.

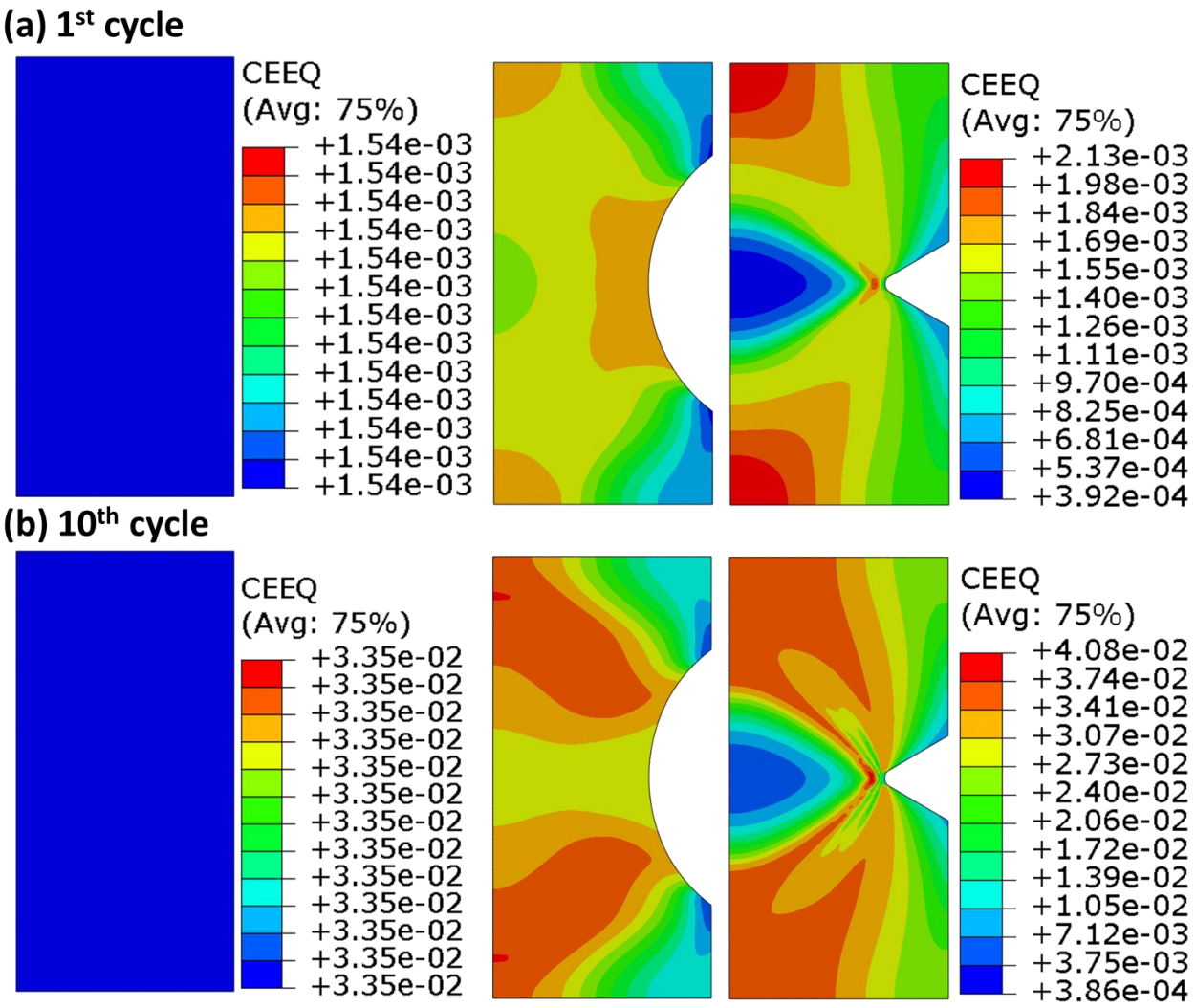

Figure 10. The contours of equivalent creep strain at the end of the hold for the uniform, shallow-notch, and V-notch specimen. (a) the 1st cycle and (b) the 10th cycle.

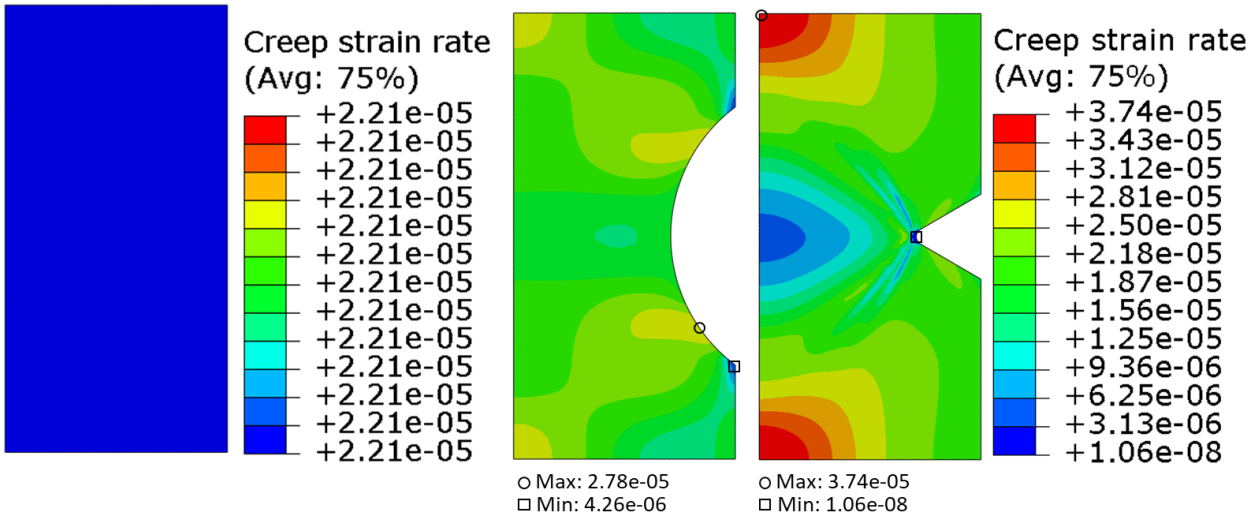

Figure 11. The contours of the average equivalent creep strain rate from the initial 10 s of the hold time at 10th cycle for the uniform, shallow-notch, and V-notch specimen.

2.3.3 DISTRIBUTION OF CALCULATED ELASTIC FOLLOW-UP FACTOR

This section describes the FE model results for elastic follow-up factor in notch specimens. A schematic of the stress strain curve of tensile-hold CF test illustrating definition of elastic follow-up factor and the mixed stress–strain controlled mode is presented in Figure 12. The elastic follow-up factor q is defined as a ratio of increased strain $\Delta\varepsilon^c$ to the elastic strain $\Delta\varepsilon^e$ during hold-time period under the uniaxial loading condition, given by Eq. (9):

$$q = \frac{\Delta\varepsilon^c}{\Delta\varepsilon^e} \tag{9}$$

Compared with the strain-controlled mode (i.e., elastic follow-up factor $q = 1$) for the uniaxial uniform specimens, discontinuous geometric shapes of notch specimens always induce the mixed stress–strain controlled mode. In this case, the elastic follow-up phenomenon contributes to the decrease of stress relaxation rate during hold time and hence the enhanced creep damage to the component. In the multiaxial stress state, the elastic follow-up factor can be calculated using Eq. (10) (Messner et al. 2019):

$$q = -\frac{\Delta W^c}{\Delta W^e} \tag{10}$$

where W^c is the creep strain energy and W^e is the elastic strain energy at hold-time period. Moreover, the magnitude of time interval in Eq. (10) reveals a difference between a tangent and a secant definition of the elastic follow-up for a structural component.

In this report, the elastic follow-up factor was calculated in each element based on Eq. (10). The q values are reported as the tangent value within the initial 10 s hold time .

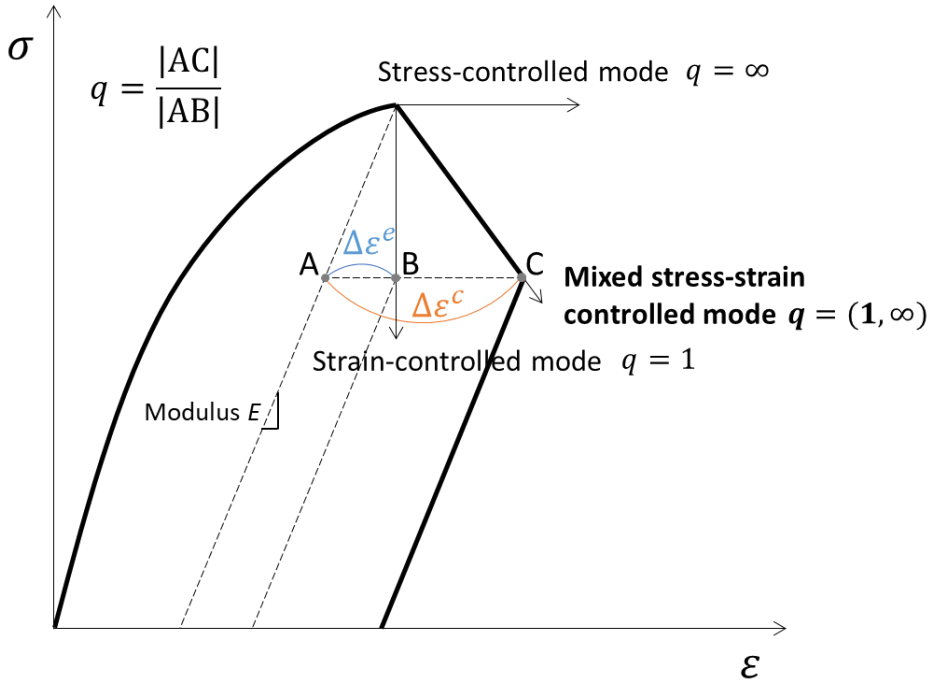

Figure 12. Schematic of the definition of elastic follow-up factor.

Figure 13 shows the elastic follow-up factor contours calculated at the 10th cycle for the uniaxial uniform, shallow-notch, and V-notch specimens of 0.5 in. gauge section and, for the 0.75 in. gauge section to quantitatively investigate the geometric effect on elastic follow-up factor. All the specimens were loaded with a nominal strain range of 0.6%. The elastic follow-up factor in both 0.5 in. and 0.75 in. gauge-length cases for the uniform specimen was distributed uniformly and equals to 1 regardless of specimen dimension. For the notch specimens, changes in the contours of elastic follow-up factor were observed when the simulated gauge length increases from 0.5 in., in Figure 13b and c, to 0.75 in., in Figure 13e and f. As the gauge length increases, the location with the maximum value in elastic follow-up factor changed, as shown in Figure 13. These changes are strongly correlated to the geometric shape and the gage length of the notch specimens, which, in turn affect stress-relaxation rate.

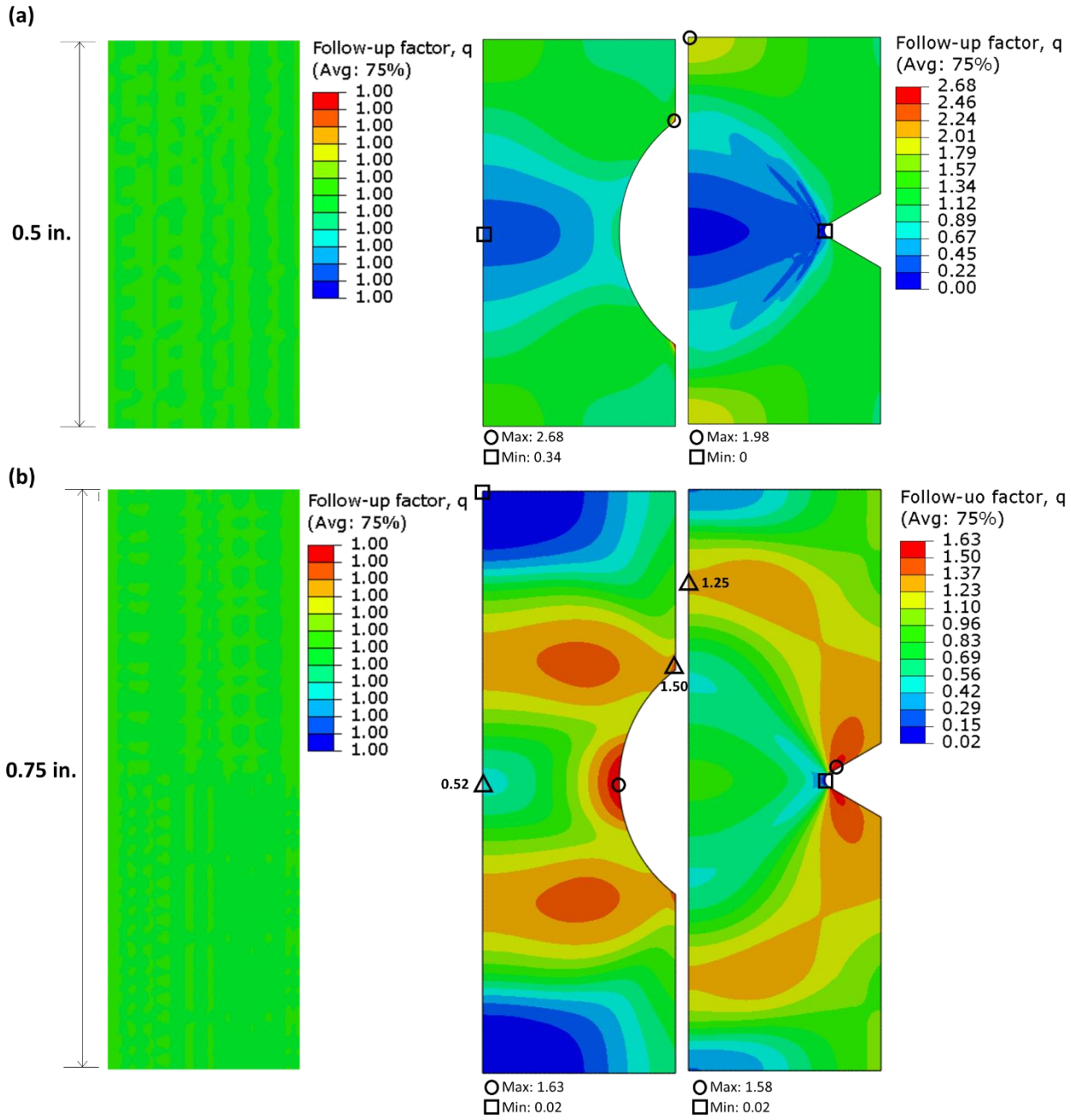

Figure 13. The contours of the average elastic follow-up factor *q* from the initial 10 s of the hold time at 10th cycle for the three specimens with (a) 0.5 in. gauge length specimens and (b) 0.75 in. gauge length.

2.3.4 MULTIAXIAL STRESS RELAXATION BEHAVIOR

The notch specimen geometry causes the multiaxial stress state and elastic follow-up phenomenon, which, in turn, influence the relaxation behavior during the hold period. To illustrate the relative changes in the stress relaxation rate, Figure 14 presents examples of the stress relaxation curves normalized by the maximum relaxation stress during the hold at the 10th cycle. Multiple locations with given stress triaxiality

factors and elastic follow-up factors for the 0.5 in. gauge length shallow-notch and V-notch specimens are shown in the plot. Clearly, the stress triaxiality factor and elastic follow-up factor both affect the stress relaxation rate. Specifically, the normalized stress relaxation curves of the uniaxial uniform specimens (stress triaxiality factor = 0.33 and elastic follow-up factor = 1) show the highest stress relaxation rate. Also, as shown in Figure 14a, the relative stress relaxation rate decreases significantly when the stress triaxiality becomes negative.

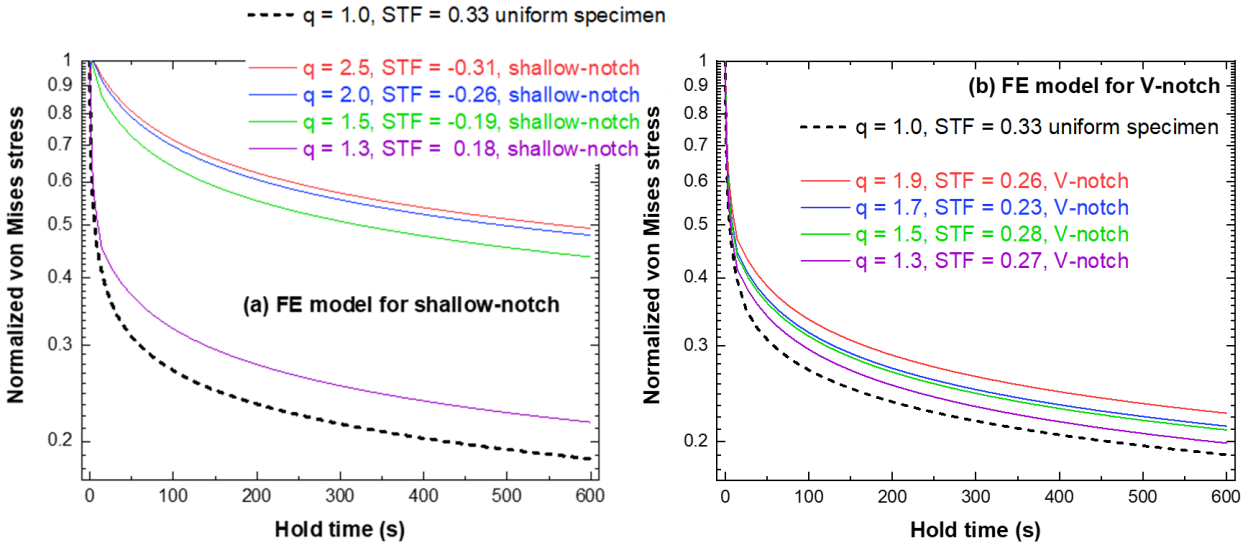

Figure 14. Examples of the normalized stress relaxation curves at the 10th cycle at various locations for the 0.5 in. gauge length for (a) shallow-notch specimen and (b) V-notch specimen.

To assess the trend in the normalized relaxation stresses with stress triaxiality factor and elastic follow-up factor and to provide better understanding of the combined effect of those factors on relaxation behavior, the contours of normalized stresses in the 0.5 in.-gauge-length notch specimens after 10 s and 100 s hold time are plotted in Figure 15 as a function of stress triaxiality factor and elastic follow-up factor. The normalized relaxation stresses in both types of notch specimens show the same trend at 10 s and 100 s hold times. The increases in elastic follow-up factor or stress triaxiality factor resulted in higher normalized relaxation stress in both notch specimens.

Figure 16 presents the general trend in the normalized relaxation stress after a 10 s hold time in the stress triaxiality factor and elastic follow-up factor space. This figure was generated by combing the data points in Figure 15a and c for the two notch geometries. Here, the stress triaxiality factor and elastic follow-up factor are assumed to be independent factors in affecting the relaxation behavior. The results demonstrate that the relaxation behavior during the hold in the CF test is strongly influenced by multiaxial stress state and elastic follow-up. The information generated from this plot can be used to assess the stresses under various CF testing conditions. For example, CF testing under compression hold (with $STF = -0.33$) would result in much higher relaxation stress than under tension hold (with $STF = 0.33$) for a uniform specimen with elastic follow up factor of 1.8, and the increase of elastic follow up would result in more significant changes in the relaxation stresses than in the tensile hold loading condition. The magnitude of

the relaxation stress will affect the CF life. Additional analysis will be performed and the inforatin collected will guide future experimental design.

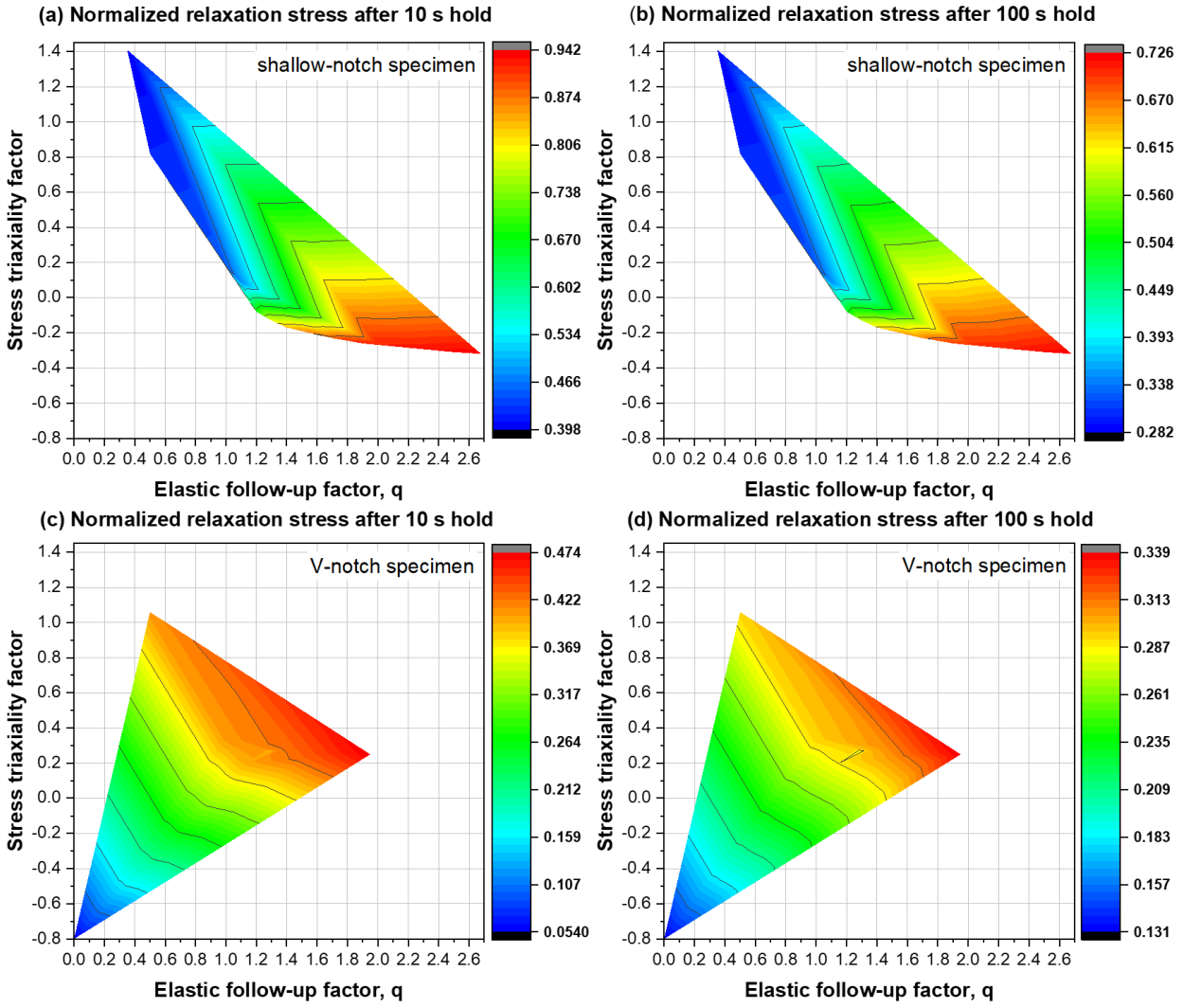

Figure 15. The normalized relaxation stresses after (a)(c) 10 s hold-time and (b)(d) 100 s hold-time as a function of stress triaxiality factor and elastic follow-up factor. (a)(b) shallow-notch specimen and (c)(d) V-notch specimen.

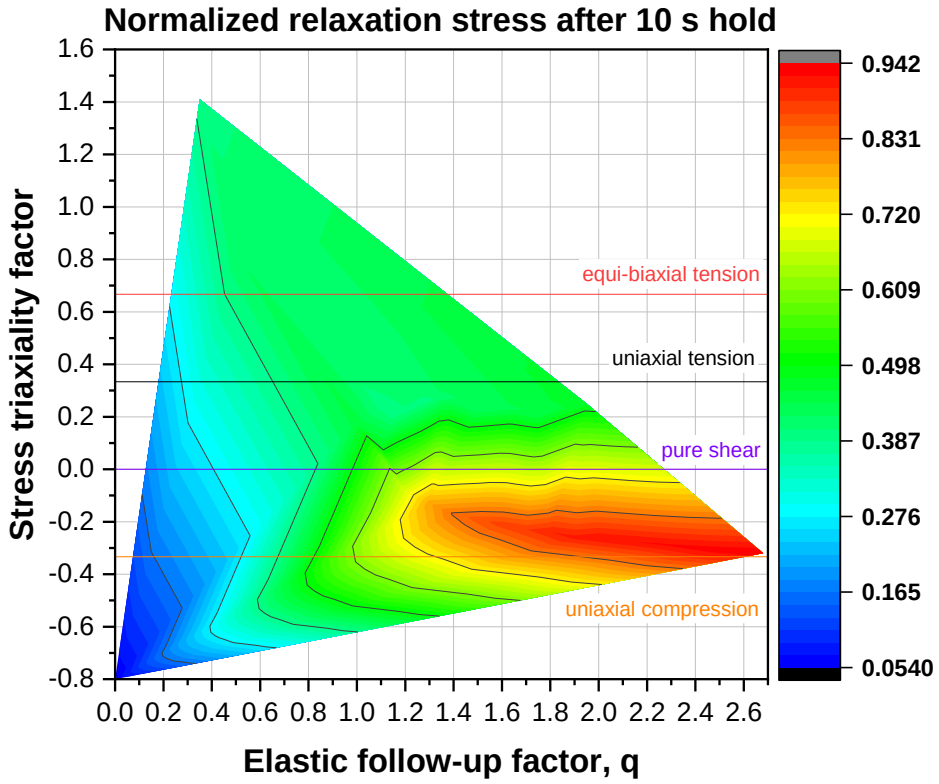

Figure 16. A combination of normalized relaxation stresses after 10 s hold time in shallow- and V-notch specimens as a function of stress triaxiality factor and elastic follow-up factor.

3. CREEP-FATIGUE EXPERIMENTS OF NOTCH SPECIMENS

The notch specimens were machined from an annealed Alloy 617 plate with heat 314626 provided by ThyssenKrupp VDM. Table 2 presents the chemical composition of this alloy plate. The specimen longitudinal direction is oriented along the rolling direction of the material plate. All the specimens are tested in the as-received, solution-annealed condition.

Table 2. The chemical composition in wt.% of Alloy 617 plate with heat number 314626

Element	C	S	Cr	Ni	Mn	Si	Mo	Ti	Cu	Fe	Al	Co	B
wt %	0.05	<0.002	22.2	54.1	0.1	0.1	8.6	0.4	0.04	1.6	1.1	11.6	<0.001

The notch specimen geometries used in this report for experimental CF tests are shown in Figure 17. Two types of specimens (i.e., shallow-notch and V-notch) were designed. To simplify the specimen machining procedure and, the notches were machined on a straight bar of total length 7.0 in. (177.8 mm) at the mid-length location. The 0.75 in. (19.0 mm) straight-gauge was mechanically polished. The straight bar section of the specimen has a diameter of 0.5 in. (6.35 mm) and the two types of notch design follows the ASTM

Standard E292-09. The ratio of the outer diameter to inner diameter in both shallow-notch and V-notch specimens is approximately $\sqrt{2}$, which is recommended by the Code of Practice (ASTM E292-09).

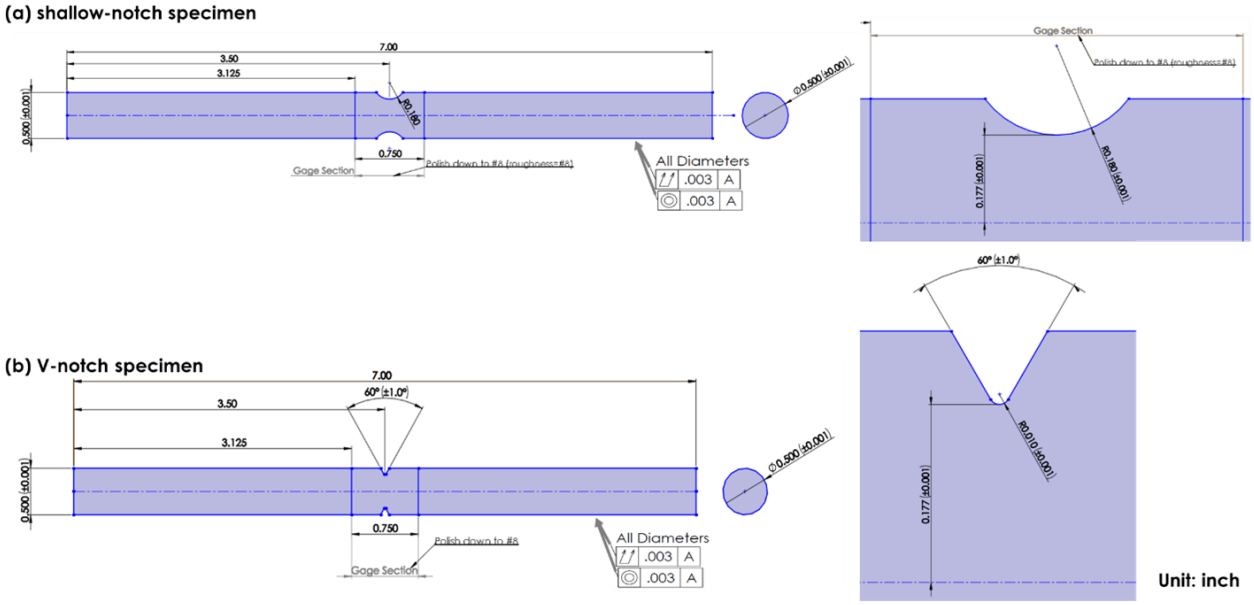

Figure 17. Notch specimens used in the CF tests at 950°C. (a) Shallow-notch and (b) V-notch specimens.

The standard CF testing procedure followed ASTM E2714-13 standard (ASTM 2013) under strain-controlled mode. The strain loading profile is shown schematically in Figure 18. It should be noted that the applied strain in CF tests is globally controlled in the section of nominal gauge length of the extensometer, as illustrated in Figure 19. Extensometers with a nominal gauge length of 0.5 in. (12.7 mm) and 0.75 in. (19.05 mm) were used to control the nominal axial strain in the gauge section. The hold-time period is applied to the maximum tensile strain amplitude. The strain profile is fully reversed. The nominal strain rate is 1×10^{-3}/s. Table 3 summaries the conditions of CF testing being conducted at ORNL.

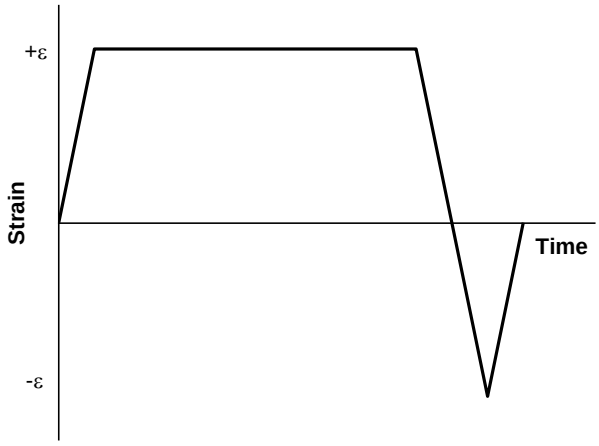

Figure 18. Strain-controlled creep-fatigue (CF) loading profile for one cycle.

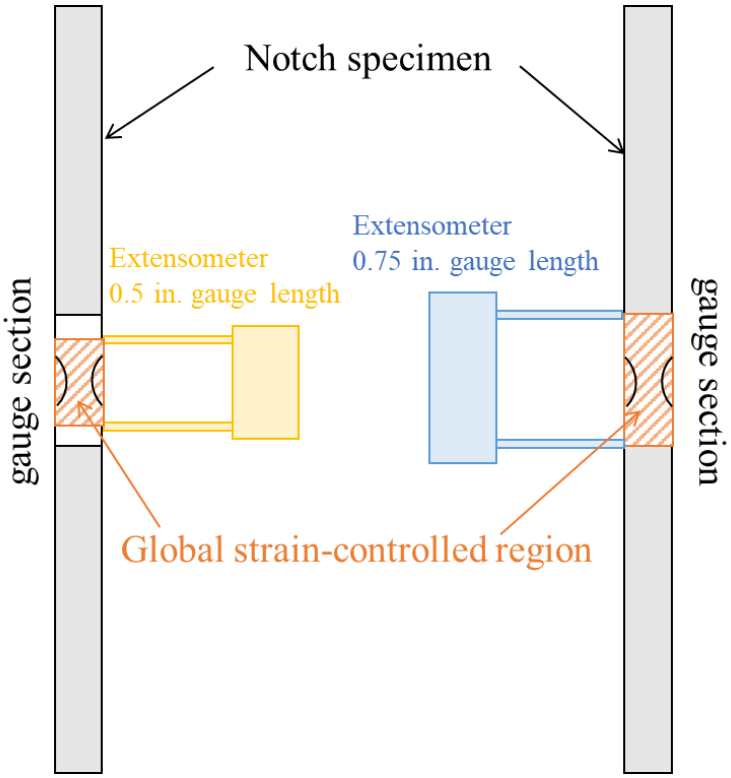

Figure 19. Schematic of the experimental CF test setup for notch specimen.

Table 3. Creep-fatigue test conditions on notch specimens for Alloy 617 at 950°C

Specimen	Test temperature (°C)	Extensometer gauge length (in.)	Nominal strain range (%)	Strain rate (/s)	Hold time (s)	Hold type
Shallow-notch	950	0.5	0.6	0.001	600	Tensile
Shallow-notch	950	0.75	0.6	0.001	600	Tensile
Shallow-notch	950	0.5	0.6	0.001	3600	Tensile
Shallow-notch	950	0.75	0.6	0.001	3600	Tensile
Shallow-notch	950	0.5	0.3	0.001	600	Tensile
V-notch	950	0.5	0.6	0.001	600	Tensile
V-notch	950	0.75	0.6	0.001	600	Tensile
V-notch	950	0.5	0.6	0.001	3600	Tensile
V-notch	950	0.75	0.6	0.001	3600	Tensile
V-notch	950	0.5	0.3	0.001	600	Tensile

4. SUMMARY

In this work, an inelastic finite element model was applied on notch Alloy 617 specimens at 950°C to provide a basic understanding of the multiaxial stress states caused by geometric discontinuities. The multiaxial stress relaxation behavior, distributions of stress triaxiality factor and elastic follow-up factor in notch specimens were calculated. The numerical results show that the stress relaxation rate is affected by both stress triaxiality factor and elastic follow-up factor. The experimental design of creep-fatigue testing on the notch specimens of Alloy 617 at 950°C was completed. Testing of the notch specimens to generate test-to-failure data is ongoing, and the results will be used to validate methods for multiaxial stress relaxation.

REFERENCES

ASTM E292-09, 2009. Standard test method for conducting time-for-rupture notch tension tests of materials. ASTM International, West Conshohocken, Pennsylvania.

ASMT E2714, "Standard Test Method for Creep-Fatigue Testing," ASTM International, West Conshohocken, Pennsylvania.

Messner, M. C., Jetter. B, and Sham, T. L. (2019), "A Method for Directly Assessing Elastic Follow Up in 3D Finite Element Calculations," Proceedings of the ASME 2019 Pressure Vessels & Piping Conference, PVP2019-93644, American Society of Mechanical Engineers, New York.

Hou, P., Sham, T.-L. and Wang, Y., (2022), "An Experimental and Analytical Study on the development of Extrapolation Method for the Creep-Fatigue Life of Alloy 617 to Low Strain Ranges and Long Hold Times at 950°C," PVP2022-84783, Proceedings of the ASME 2022 Pressure Vessels & Piping Conference, July 17-22, 2022, Las Vegas, Nevada, USA

Wang, Y., Jetter, R. I., and Sham, T.-L. (2016a), "FY16 Progress Report on Test Results In Support Of Integrated EPP and SMT Design Methods Development" ORNL/TM-2016/330, Oak Ridge National Laboratory, Oak Ridge, Tennessee.

Wang, Y., Jetter, R. I., and Sham, T.-L. (2016b), "Preliminary Test Results in Support of Integrated EPP and SMT Design Methods Development," ORNL/TM-2016/76, Oak Ridge National Laboratory, Oak Ridge, Tennessee.

Wang, Y., Jetter, R.I., and Sham, T.-L. (2017a), "Report on FY17 Testing in Support of Integrated EPP-SMT Design Methods Development," ORNL/TM-2017/351, Oak Ridge National Laboratory, Oak Ridge, Tennessee.

Wang, Y., Jetter, and Sham, T.-L. (2017b), "Pressurized Creep-Fatigue Testing of Alloy 617 Using Simplified Model Test Method," Proceedings of the ASME 2017 Pressure Vessels and Piping Conference, PVP2017-65457, American Society of Mechanical Engineers, New York.

Wang, Y., Jetter, R. I., Messner, M., and Sham, T.-L. (2018), "Report on FY18 Testing Results in Support of Integrated EPP-SMT Design Methods Development," ORNL/TM-2018/887, Oak Ridge National Laboratory, Oak Ridge, Tennessee.

Wang, Y., Jetter, R. I., Messner, M., and Sham, T.-L. (2019), "Development of Simplified Model Test Method for Creep-fatigue Evaluation," Proceedings of the ASME 2019 Pressure Vessels and Piping Conference, PVP2019-93648, American Society of Mechanical Engineers, New York.

Wang, Y., Hou, P., Jetter, R. I., and Sham, T.-L. (2020), "Report on FY2020 Test Results in Support of the Development of EPP Plus SMT Design Method," ORNL/TM-2020/1620, Oak Ridge National Laboratory, Oak Ridge, Tennessee.

Wang, Y., Hou, P., Jetter, R. I., and Sham, T.-L. (2021a), "Evaluation of the Primary-Load Effects on Creep-Fatigue Life of Alloy 617 Using Simplified Model Test Method," Proceedings of the ASME 2021 Pressure Vessels and Piping Conference, PVP2021-61658, American Society of Mechanical Engineers, New York.

Wang, Y., Hou, P., Jetter, R. I., and Sham, T.-L. (2021b), "Report on FY2021 Test Results in Support of the Development of EPP Plus SMT Design Method," ORNL/TM-2021/2159, Oak Ridge National Laboratory, Oak Ridge, Tennessee.

Wang, Y., Hou, P., and Sham, T.-L. (2022b), "An Extrapolation Method for Strain Ranges and Hold Times in Developing the EPP+SMT Creep-Fatigue Design Curves for Alloy 617," ORNL/TM-2022/2517, Oak Ridge National Laboratory, Oak Ridge, Tennessee.

Wright, R.N. (2021), "Draft ASME Boiler and Pressure Vessel Code Cases and Technical Bases for Use of Alloy 617 for Construction of Nuclear Components Under Section Ill, Division 5," INL/EXT-15-36305 Revision 2, Idaho National Laboratory, Idaho Falls, Idaho.

Page intentionally left blank.